

# Finite element based form-finding algorithm for tensegrity structures

M. Pagitz<sup>a</sup>, J.M. Mirats Tur<sup>b,\*</sup>

<sup>a</sup> Department of Engineering, University of Cambridge, Trumpington Street, Cambridge CB2 1PZ, UK

<sup>b</sup> Institut de Robòtica i Informàtica Industrial (CSIC-UPC), C/Llorens i Artigas 4-6, Barcelona 08028, Spain

## A B S T R A C T

This paper presents a novel form-finding algorithm for tensegrity structures that is based on the finite element method. The required data for the form-finding is the topology of the structure, undeformed bar lengths, total cable length, prestress of cables and stiffness of bars. The form-finding is done by modifying the single cable lengths such that the total cable length is preserved and the potential energy of the system is minimized. Two- and three-dimensional examples are presented that demonstrate the excellent performance of the proposed algorithm.

Keywords:  
Tensegrity  
Form-finding

## 1. Introduction

A tensegrity is a structure that maintains its shape by using a *discontinuous* set of compressive elements (bars) that are connected to a *continuous* net of prestressed tensile elements (cables), Pugh (1976). Hence, the word *tensegrity* is an abbreviation for *tensile integrity*, Fuller (1962). Although tensegrities were first created within the art community, Snelson (1965), they have been rapidly applied to other disciplines such as architecture, Hanaor (1992), and space engineering, Tibert (2003). Fig. 1 shows an example of a tensegrity structure.

This paper is concerned with the form-finding of tensegrity structures on the basis of the finite element method. A novel algorithm is presented that can be used to find tensegrity configurations for topologies that are statically indeterminate, statically determinate or even kinematic. The paper is organized as follows: Section 2 reviews the literature and Section 3 introduces the theoretical foundation of the proposed method. Section 4 presents form-finding results and convergence plots for different two- and three-dimensional examples. Section 5 discusses the application of the proposed method to kinematic and statically determinate topologies on the basis of symmetry transformation matrices. Finally, Section 6 concludes the paper.

## 2. Literature review

The first methods for constructing simple and highly symmetric tensegrities were based on convex polyhedra and published by Fuller (1975), Emmerich (1988) and Snelson (1965). However, it was

found that the resulting shapes were not identical to the corresponding polyhedra so that it became necessary to develop new form-finding methods. A comprehensive review about the form-finding of tensegrities can be found in Tibert and Pellegrino (2003). Existing form-finding algorithms can be classified into *kinematical* and *statical methods*:

*Kinematical methods* increase (decrease) the length of bars (cables) until a maximum (minimum) is reached while the length of cables (bars) is kept constant. For example, Connelly and Terrel (1995) proposed an analytical method where the coordinates of each node are expressed as a function of geometric parameters. Starting from an arbitrary configuration they maximized (minimized) the length of bars (cables) for given cable (bar) lengths. Although this approach can be used for highly symmetric structures, it becomes infeasible for non-symmetric tensegrities due to the large number of variables that are required to describe a general configuration. Other methods that fall into this category are, for example, Pellegrino (1986) and Belkacem (1987).

*Statical methods* minimize the potential energy of the tensegrity by considering one or more constraints. For example, Kenner (2003) used node equilibrium conditions and symmetry arguments to find stable configurations of some simple tensegrities. Linkwitz (1999) and Schek (1974) developed the force density method that requires prior knowledge of the stress coefficients for all members. Masic et al. (2005) presented a modified version of the force density method that explicitly includes shape constraints. Connelly (1993) published a form-finding method that assigns an energy function to a tensegrity and searches the minimum of this function. It was shown that the latter method is closely related to the force density method. An approach by Sultan et al. (1999) identifies a set of generalized coordinates for a particular tensegrity framework and uses symbolic manipulation to obtain the equilibrium matrix. However, general results are hard to find so that only some

\* Corresponding author. Tel: +34 934015752; fax: +34 934015750.  
E-mail address: jmirats@iri.upc.edu (J.M. Mirats Tur).

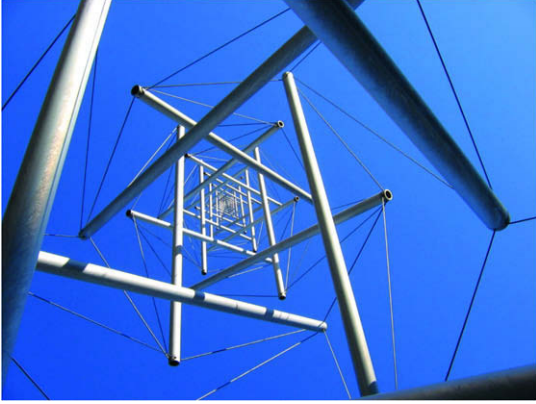


Fig. 1. Tensegrity structure (Needle tower by Kenneth Snelson, courtesy Wikipedia).

solutions for highly symmetric tensegrities have been given, Sultan (1999). Finally, Estrada et al. (2006) published an algorithm where the force density for each member is iteratively calculated by using rank constraints on the stress and rigidity matrices.

### 3. Theoretical framework

In the following we consider only statically indeterminate topologies. The form-finding for topologies that are statically determinate or kinematic is discussed in Section 5. The proposed form-finding algorithm is outlined in Fig. 2. The required data are the topology of the structure (i.e. the connectivity of bar and cable elements), undeformed bar lengths, total cable length, prestress of cables and stiffness of bars. Note that the initial cable lengths can be chosen arbitrarily as long as they satisfy the total cable length.

The algorithm splits naturally into *two stages*:

- *Stage 1* computes an equilibrium configuration of a structure with elastic bars and given cable lengths. Furthermore, first and second order information is computed at the equilibrium configuration that relates the change of bar lengths to the change of cable lengths.
- *Stage 2* is based on the first and second order information from *Stage 1* and assumes elastic bars and prestressed cables that

have zero axial stiffness. This stage modifies the single cable lengths by simultaneously preserving the total cable length such that the energy of the system is minimized.

The algorithm iterates between both stages until a tensegrity is found. Note that there are, depending on the spatial dimension,  $2n_n$  or  $3n_n$  degrees of freedom in the first stage and only  $n_c + 1$  degrees of freedom in the second stage ( $n_n$  is the number of nodes and  $n_c$  the number of cables). A detailed presentation of both stages is given in the following subsections.

#### 3.1. The first stage

Stage 1 computes an equilibrium configuration of a structure with elastic bars and given cable lengths by using the finite element method. The cables and bars are modeled with the geometric nonlinear two-node bar finite element that is presented in Appendix A. The initial cable lengths are preserved by defining

$$E^c A^c \gg E^b A^b \quad (1)$$

where  $E^c A^c$  is the axial stiffness of the cables and  $E^b A^b$  the axial stiffness of the bars. The total energy  $\Pi$  of the system can be written as

$$\Pi = \Pi^c + \Pi^b = \sum_{i=1}^{n_c} \frac{L_0^{c_i}}{2E^c A^c} f^{c_i,2} + \sum_{i=1}^{n_b} \frac{L_0^{b_i}}{2E^b A^b} f^{b_i,2} \quad (2)$$

where  $f$  are the element forces. Note that the energy of the cables is negligible for finite cable forces since  $E^c A^c \gg E^b A^b$ . Therefore, we can conclude that the first stage computes an equilibrium configuration that minimizes the energy of the bars for given cable lengths.

The second stage of the algorithm requires, at the previously obtained equilibrium configuration, first and second order information that relates the change of bar lengths to the change of cable lengths. In particular, we need the gradient matrix  $\mathbf{G}$  of size  $n_b \times n_c$

$$\mathbf{G} = \begin{bmatrix} \frac{\partial L^{b_1}}{\partial L^{c_1}} & \dots & \frac{\partial L^{b_1}}{\partial L^{c_{n_c}}} \\ \vdots & \ddots & \vdots \\ \frac{\partial L^{b_{n_b}}}{\partial L^{c_1}} & \dots & \frac{\partial L^{b_{n_b}}}{\partial L^{c_{n_c}}} \end{bmatrix} \quad (3)$$

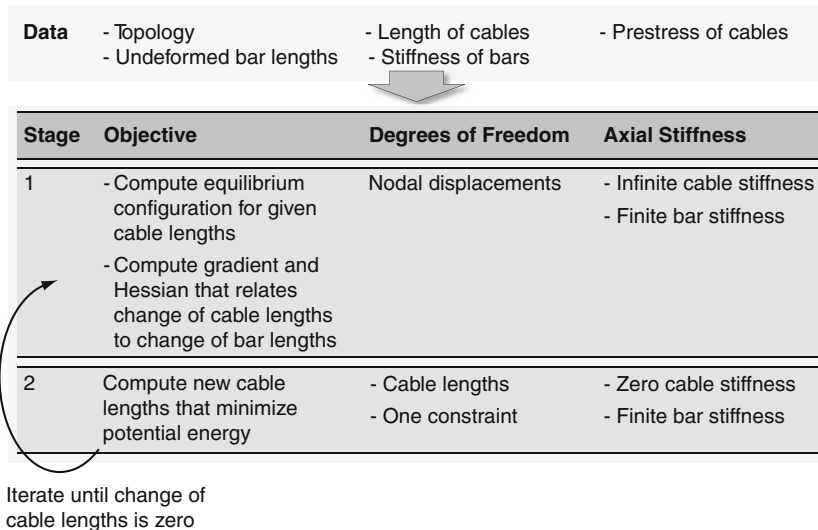


Fig. 2. Schematic drawing of proposed form-finding algorithm.

and the Hessian  $\mathbf{H}$  of size  $n_b \times n_c \times n_c$

$$\mathbf{H} = \begin{bmatrix} \frac{\partial^2 L^{b_1}}{\partial L^{c_1} \partial L^{c_1}} & \cdots & \frac{\partial^2 L^{b_1}}{\partial L^{c_1} \partial L^{c_{n_c}}} \\ \vdots & \ddots & \vdots \\ \frac{\partial^2 L^{b_1}}{\partial L^{c_{n_c}} \partial L^{c_1}} & \cdots & \frac{\partial^2 L^{b_1}}{\partial L^{c_{n_c}} \partial L^{c_{n_c}}} \end{bmatrix} \cdots \begin{bmatrix} \frac{\partial^2 L^{b_{n_b}}}{\partial L^{c_1} \partial L^{c_1}} & \cdots & \frac{\partial^2 L^{b_{n_b}}}{\partial L^{c_1} \partial L^{c_{n_c}}} \\ \vdots & \ddots & \vdots \\ \frac{\partial^2 L^{b_{n_b}}}{\partial L^{c_{n_c}} \partial L^{c_1}} & \cdots & \frac{\partial^2 L^{b_{n_b}}}{\partial L^{c_{n_c}} \partial L^{c_{n_c}}} \end{bmatrix} \quad (4)$$

These matrices are computed by using a forward finite difference (FFD) scheme and cable increments that are a multiple of  $\Delta L_{\text{FFD}}^c$ . A pseudo-code of the first stage is given in Algorithm 1.

### 3.2. The second stage

Stage 2 modifies the single cable lengths by simultaneously preserving the total cable length such that the energy of the system is minimized. The second stage is based on the gradient  $\mathbf{G}$  and the Hessian  $\mathbf{H}$  from Stage 1. Furthermore, the properties of the bars are unchanged compared to the first stage. However, the cables possess now a prestress  $\sigma^c$  but no axial stiffness  $E^c A^c$  so that the potential energy  $\Pi^{\text{tens}}$  of a tensegrity is

$$\begin{aligned} \Pi^{\text{tens}} &= \sum_{i=1}^{n_c} A^{c_i} \sigma^{c_i} (L^{c_i} - L_0^{c_i}) + \sum_{i=1}^{n_b} E^{b_i} A^{b_i} \int_{L_0^{b_i}}^{L^{b_i}} \frac{L^{b_i^2} - L_0^{b_i^2}}{2L_0^{b_i^2}} dL^{b_i} \\ &= \sum_{i=1}^{n_c} A^{c_i} \sigma^{c_i} (L^{c_i} - L_0^{c_i}) + \sum_{i=1}^{n_b} E^{b_i} A^{b_i} \left( \frac{L^{b_i^3} - L_0^{b_i^3}}{6L_0^{b_i^2}} - \frac{L^{b_i} - L_0^{b_i}}{2} \right) \end{aligned} \quad (5)$$

where superscript  $c_i$  refers to the  $i$ th cable and  $b_i$  to the  $i$ th bar. The force vector of the tensegrity can be written as

$$\frac{\partial \Pi^{\text{tens}}}{\partial L^{c_i}} = A^{c_i} \sigma^{c_i} + \sum_{i=1}^{n_b} E^{b_i} A^{b_i} \frac{L^{b_i^2} - L_0^{b_i^2}}{2L_0^{b_i^2}} \frac{\partial L^{b_i}}{\partial L^{c_i}} \quad (6)$$

where the derivatives  $\partial L^{b_i} / \partial L^{c_j}$  are known from Stage 1. Note that the forces are in the direction of the cables since the force vector is the derivative of the potential energy with respect to the cable lengths. Finally, the tensegrity stiffness matrix results in

$$\frac{\partial^2 \Pi^{\text{tens}}}{\partial L^{c_j} \partial L^{c_k}} = \mathbf{K}^{\text{tens}} = \sum_{i=1}^{n_b} E^{b_i} A^{b_i} \left( \underbrace{\frac{L^{b_i}}{L_0^{b_i^2}} \frac{\partial L^{b_i}}{\partial L^{c_j}} \frac{\partial L^{b_i}}{\partial L^{c_k}}}_{\text{Material stiffness}} + \underbrace{\frac{L^{b_i^2} - L_0^{b_i^2}}{2L_0^{b_i^2}} \frac{\partial^2 L^{b_i}}{\partial L^{c_j} \partial L^{c_k}}}_{\text{Geometric stiffness}} \right) \quad (7)$$

The total cable length is preserved by augmenting the stiffness matrix  $\mathbf{K}^{\text{tens}}$  with a linear constraint

$$\begin{bmatrix} \Delta f^{c_1} \\ \vdots \\ \Delta f^{c_{n_c-1}} \\ \Delta f^{c_{n_c}} \\ 0 \end{bmatrix} = \begin{bmatrix} \mathbf{K}^{\text{tens}} & \begin{matrix} 1 \\ \vdots \\ 1 \\ 1 \\ 0 \end{matrix} \\ \hline 1 & \cdots & 1 & 1 & 0 \end{bmatrix} \begin{bmatrix} \Delta L^{c_1} \\ \vdots \\ \Delta L^{c_{n_c-1}} \\ \Delta L^{c_{n_c}} \\ \lambda \end{bmatrix} \quad (8)$$

A closer look at Eq. (7) reveals that the stiffness matrix  $\mathbf{K}^{\text{tens}}$  is exclusively based on bar related terms so that the geometric stiffness matrix disappears and the material stiffness matrix becomes singular for  $L^{b_i} = L_0^{b_i}$ . This can be avoided by choosing a sufficiently small total cable length at the start of the simulation. Furthermore, the first few iteration steps of the form-finding are generally large. Therefore, it is advisable to limit the maximum step size or to implement a line search algorithm like, for example, the golden section method, Vanderplaats (2001). Throughout this paper, the maximum change of a single cable length was constrained to  $\Delta L_{\text{max}}^c$ . A pseudo-code of the proposed form-finding method is given in Algorithm 2.

**Table 1**

Geometric, material and algorithm parameters for two-dimensional examples.

	$A^b E^b$	$A^c E^c$	$A^c \sigma^c$	$\Delta L_{\text{FFD}}^c$	$\Delta L_{\text{max}}^c$
Stage 1	1	$10^6$	$A^c E^c \sigma_G^c$	$10^{-4}$	–
Stage 2	1	0	1	–	0.5

**Algorithm 1.** Pseudo-code of Stage 1.

**Data:** Topology,  $L_0^b$ ,  $L^c$ ,  $E^b A^b$ ,  $\Delta L_{\text{FFD}}^c$

**Result:** Equilibrium configuration for  $L^c$ ,  $\mathbf{G}$  and  $\mathbf{H}$

repeat

    Compute residual force vector  $\mathbf{p}$

    while  $|\mathbf{p}| > 1e-7$  do

        Compute stiffness matrix  $\mathbf{K}$

        Solve  $-\mathbf{p} = \mathbf{K} \Delta \mathbf{u}$  ( $2n_n$  or  $3n_n$  degrees of freedom)

        Update displacements ( $\mathbf{u} = \mathbf{u} + \Delta \mathbf{u}$ )

        Compute residual force vector  $\mathbf{p}$

    end

    Increase/decrease cable lengths by multiples of  $\Delta L_{\text{FFD}}^c$

until all data for  $\mathbf{G}$  and  $\mathbf{H}$  is obtained ;

Compute gradient  $\mathbf{G}$  and Hessian  $\mathbf{H}$  at equilibrium configuration

**Algorithm 2.** Pseudo-code of proposed form-finding method.

**Data:** Topology,  $L_0^b$ ,  $L^c$ ,  $E^b A^b$ ,  $A^c \sigma^c$ ,  $\Delta L_{\text{FFD}}^c$ ,  $\Delta L_{\text{max}}^c$

**Result:** Tensegrity

Call Algorithm 1

Compute residual force vector  $\mathbf{p}^{\text{tens}}$

while  $|\mathbf{p}^{\text{tens}}| > 1e-7$  do

    Compute stiffness matrix  $\mathbf{K}^{\text{tens}}$

    Solve  $-\mathbf{p}^{\text{tens}} = \mathbf{K}^{\text{tens}} \Delta L^c$  ( $n_c + 1$  degrees of freedom)

    Limit maximum change of cable length to  $\Delta L_{\text{max}}^c$

    Update cable lengths ( $L^c = L^c + \Delta L^c$ )

    Call Algorithm 1

    Compute residual force vector  $\mathbf{p}^{\text{tens}}$

end

Plot tensegrity

## 4. Examples

This section presents two- and three-dimensional examples that demonstrate the form-finding and convergence properties of the proposed algorithm.

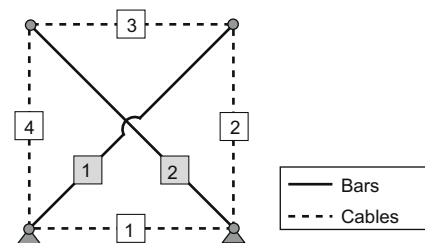


**Fig. 3.** Topology and element numbering of two-dimensional examples.

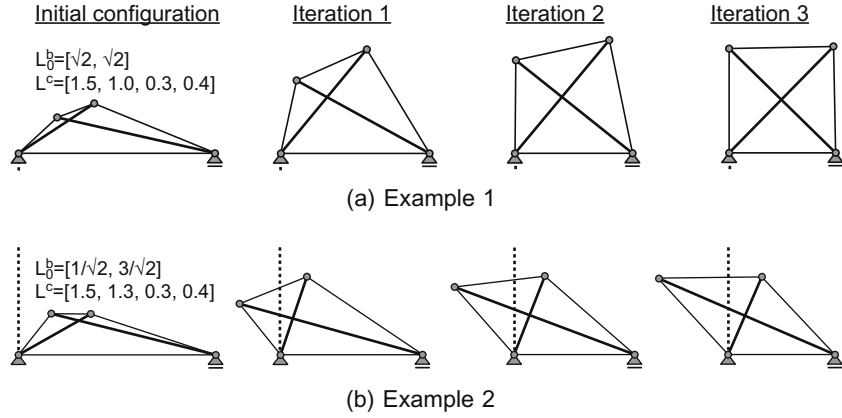


Fig. 4. Initial configurations and first three iterations of two-dimensional examples.

#### 4.1. Two-dimensional examples

The geometric, material and algorithm parameters for the two-dimensional examples are summarized in Table 1. Note that  $\Delta L_{\text{FFD}}^c$  is the step size for the forward finite difference scheme to compute (3) and (4). Furthermore,  $\Delta L_{\text{max}}^c$  is the maximum change of a single cable length during an iteration.

The topology and element numbering for both examples is given in Fig. 3. Fig. 4 shows the initial configurations and the first three iterations. The initial configuration is a stable equilibrium for given cable lengths  $L^c$  and undeformed bar lengths  $L_0^b$ . It can be seen that the first example converges to a square and the second example to a rhombus after only three iterations. Note that the total cable length of the square/rhombus is identical to the total cable length of the corresponding initial configurations.

Fig. 5 shows the convergence of

$$|\Delta L^c| = \sqrt{\Delta L^{c_1^2} + \dots + \Delta L^{c_n^2}} \quad (9)$$

and the Lagrange multiplier  $\lambda$  for a maximum step size of  $\Delta L_{\text{max}}^c = 0.5$ . Note that the effective cable forces are  $A^{c_i} \sigma^{c_i} + \lambda$  so that the bars are unstressed for  $\lambda = -1$ . Therefore, if  $\lambda \rightarrow -1$  it is necessary to decrease the total cable length in order to avoid a singular stiffness matrix.

#### 4.2. Three-dimensional examples

The geometric and material properties as well as the algorithm parameters for the three-dimensional examples are summarized in Table 2. The topology and the element numbering is given in Fig. 6. Since the bars describe two independent tetrahedrons it was decided to use this representation in order to simplify the interpretation of the figures.

Table 2

Geometric, material and algorithm parameters for three-dimensional examples.

	$A^b E^b$	$A^c E^c$	$A^c \sigma^c$	$\Delta L_{\text{FFD}}^c$	$\Delta L_{\text{max}}^c$
Stage 1	1	$10^5$	$A^c E^c \sigma_G^c$	$10^{-4}$	-
Stage 2	1	0	1	-	0.25

Fig. 7 shows four different initial configurations and the resulting tensegrities. Note that all tensegrities have the same topology, total cable length and undeformed bars. It can be seen that the final result depends heavily on the initial configuration. Furthermore, the initial equilibrium configuration for a given set of cable lengths is generally not unique. The high degree of symmetry of the presented tensegrities is driven by the assumption of uniform bar lengths and cable forces. However, the proposed algorithm is capable of finding tensegrities for arbitrary bar lengths and cable forces.

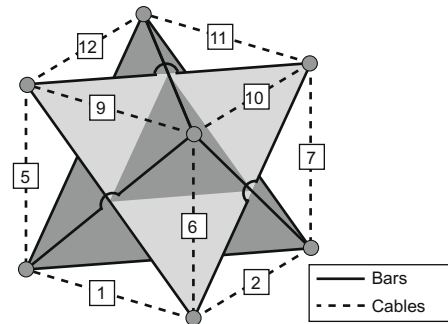


Fig. 6. Topology and element numbering of three-dimensional examples.

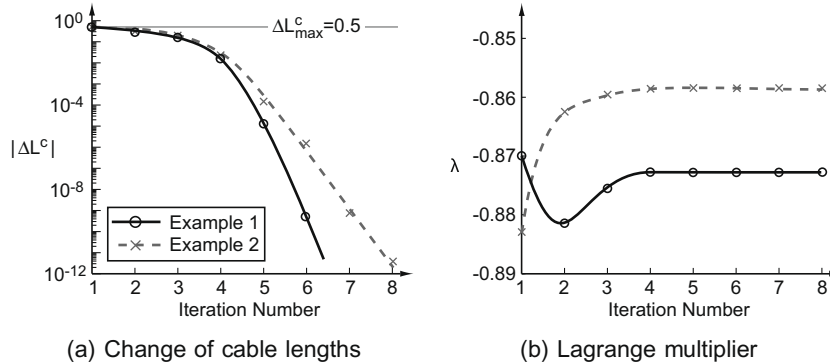


Fig. 5. Convergence of two-dimensional examples.

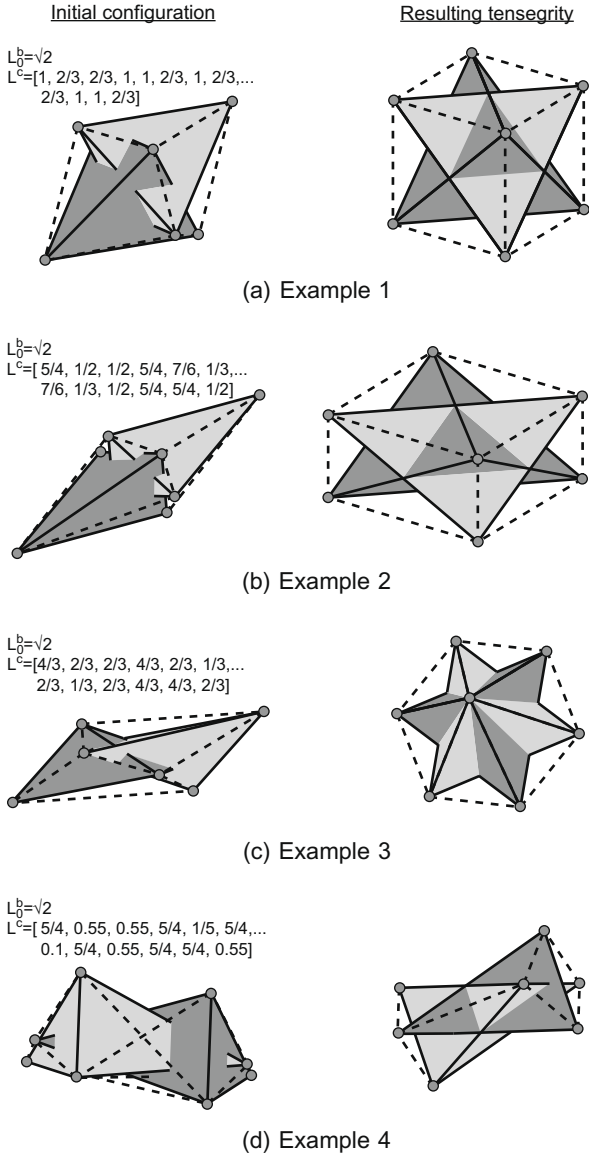


Fig. 7. Initial configurations and resulting tensegrities of three-dimensional examples. Note that, for all examples,  $\sum_{i=1}^{n_c} L^i = 10$ .

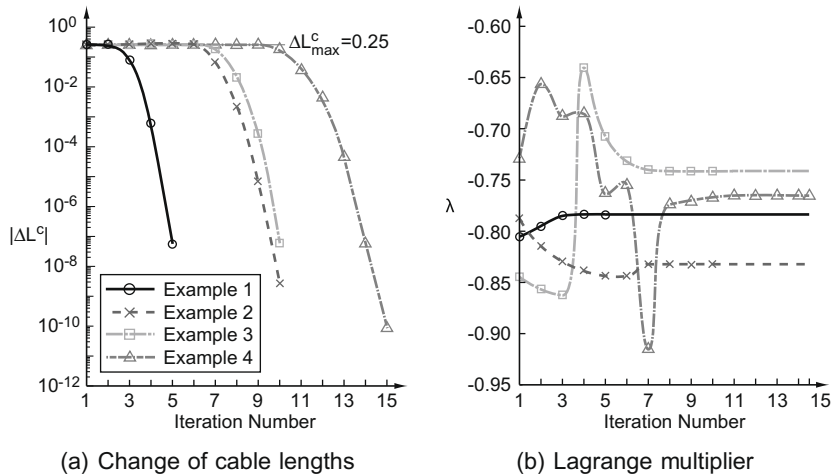


Fig. 8. Convergence of three-dimensional examples.

Fig. 8 shows the convergence of the three-dimensional examples for  $\Delta L_{\max}^c = 0.25$ .

## 5. Tensegrities and symmetry

Previous examples have in common that their topologies are statically indeterminate. Therefore,

$$dn_n - n_e - n_s = k < 0 \quad (10)$$

where  $d$  is the spatial dimension,  $n_n$  the number of nodes,  $n_e$  the number of elements,  $n_s$  the number of supports ( $n_s = 6$  for  $d = 3$  and  $n_s = 3$  for  $d = 2$ ) and  $-k$  are the states of self stress.

However, there exists a great number of tensegrities where  $k \geq 0$ . A general property of such tensegrities is that they possess a high degree of symmetry. Since these structures are statically determinate,  $k = 0$ , or even kinematic,  $k > 0$ , it is not possible to directly apply the previously introduced algorithm. Instead it is necessary to constrain these structures by assuming a certain symmetry group (by enforcing symmetry we indirectly increase  $n_s$ ). This can be done by transforming the stiffness matrices of the first and second stage (see Fig. 2) into symmetry space by using transformation matrices that were introduced by Pagitz and James (2007). Since these transformation matrices are based on Fourier series and vector spherical harmonics it is possible to construct them purely from geometric arguments. Hence, no group theory is required. An example for the block diagonalization of large stiffness matrices can be found in Pagitz and Pellegrino (2007).

## 6. Conclusions

We presented a novel numerical method for the form-finding of tensegrity structures that is based on the finite element method. The proposed algorithm reduces the solution space, depending on the spatial dimension, from  $2n_n$  or  $3n_n$  to  $n_c + 1$  degrees of freedom where  $n_n$  is the number of nodes and  $n_c$  the number of cables. As a result, the form-finding only requires a linear constraint so that a deep understanding of the form-finding process itself is obtained. It was demonstrated that the method converges within a few iterations from highly distorted initial configurations to a tensegrity. Finally, it was discussed how symmetry transformation matrices can be used to find tensegrity configurations that are statically determinate or kinematic.

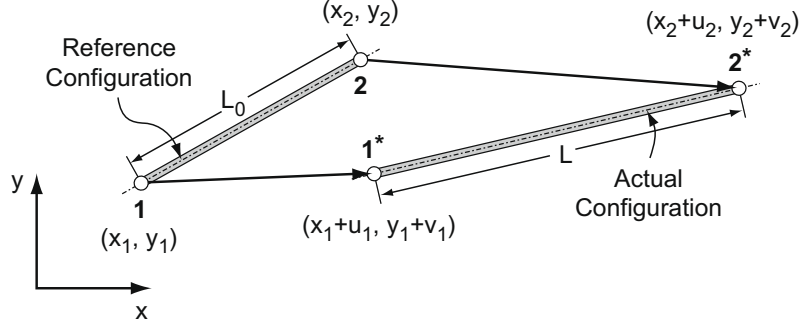


Fig. A.1. Global cartesian coordinate system of bar element in two dimensions.

## Acknowledgments

Markus Pagitz is a Research Fellow at St. John's College Cambridge. Josep M. Mirats Tur thanks the Education and Science Ministry of the Spanish Government for partially financing this work by means of where project PROFIT CIT-020400-2007-78.

## Appendix A. Nonlinear bar finite element

This appendix provides a brief derivation of a two-node geometric nonlinear bar finite element that is used in the first stage of the proposed algorithm.

Several different strain measures are used in mechanics. The most well known is the so-called engineering strain

$$\varepsilon_E = \frac{L - L_0}{L_0} \quad (\text{A.1})$$

where  $L_0$  is the undeformed and  $L$  the deformed bar length, Fig. A.1. This measure has the advantage that the strain  $\varepsilon_E$  is proportional to the change of bar length. The engineering strain is based on radicals since the bar lengths

$$L_0 = \sqrt{x_{21}^2 + y_{21}^2 + z_{21}^2};$$

$$L = \sqrt{(x_{21} + u_{21})^2 + (y_{21} + v_{21})^2 + (z_{21} + w_{21})^2} \quad (\text{A.2})$$

are computed from nodal coordinates where, for example,  $x_{21} = x_2 - x_1$ . Strain measures that avoid these radicals are often used in order to simplify the derivation of finite elements. One of the most well known is the Green-Lagrange strain measure

$$\varepsilon_G = \frac{L^2 - L_0^2}{2L_0^2} \quad (\text{A.3})$$

It should be noted that both strain measures have the same tangent for infinitesimally small deformations. For the sake of simplicity we will use the Green-Lagrange strain in the following.

The energy  $\Pi$  of a bar without prestress is

$$\Pi = EA \int_{L_0}^L \varepsilon_G(L) dL = EA \left( \frac{L^3 - L_0^3}{6L_0^2} - \frac{L - L_0}{2} \right) \quad (\text{A.4})$$

so that the internal force vector  $\mathbf{p} = \partial\Pi/\partial\mathbf{u}$  results in

$$\mathbf{p} = \frac{EA}{L} \varepsilon_G [-a_x \quad -a_y \quad -a_z \quad a_x \quad a_y \quad a_z]^T$$

$$\approx \frac{EA}{L_0} \varepsilon_G [-a_x \quad -a_y \quad -a_z \quad a_x \quad a_y \quad a_z]^T \quad (\text{A.5})$$

where  $\mathbf{u}$  are the nodal displacements and, for example,  $a_x = x_{21} + u_{21}$ . Finally, the stiffness matrix  $\mathbf{K} = \partial\mathbf{p}/\partial\mathbf{u}$  is

$$\mathbf{K} \approx \frac{EA}{L_0^3} \begin{bmatrix} a_x^2 & a_x a_y & a_x a_z & -a_x^2 & -a_x a_y & -a_x a_z \\ & a_y^2 & a_y a_z & -a_x a_y & -a_y^2 & -a_y a_z \\ & & a_z^2 & -a_x a_z & -a_y a_z & -a_z^2 \\ \text{Sym.} & & & a_x^2 & a_x a_y & a_x a_z \\ & & & & a_y^2 & a_y a_z \\ & & & & & a_z^2 \end{bmatrix}$$

$$+ \frac{EA}{L_0} \varepsilon_G \begin{bmatrix} 1 & 0 & 0 & -1 & 0 & 0 \\ & 1 & 0 & 0 & -1 & 0 \\ & & 1 & 0 & 0 & -1 \\ \text{Sym.} & & & 1 & 0 & 0 \\ & & & & 1 & 0 \\ & & & & & 1 \end{bmatrix} \quad (\text{A.6})$$

## References

- Belkacem, S., 1987. Recherche de forme par relaxation dynamique des structures reticulées spatiales autocontraintes, Ph.D. Thesis, L' Université Paul Sabatier de Toulouse.
- Connelly, R., 1993. Handbook of Convex Geometry. Elsevier, Amsterdam. Chapter: Rigidity.
- Connelly, R., Terrel, M., 1995. Globally rigid symmetric tensegrities. Journal of Structural Topology 21, 59–78.
- Emmerich, D., 1988. Structures tendues et autotendantes, Editions de l'Ecole d'Architecture de Paris La Villette.
- Estrada, G.G., Bungartz, H.J., Mohrdieck, C., 2006. Numerical form-finding of tensegrity structures. International Journal of Solids and Structures 43 (22–23), 6855–6868.
- Fuller, R.B., 1962. Tensile-Integrity Structures, United States Patent 3063521.
- Fuller, R.B., 1975. Synergetics: Explorations in the Geometry of Thinking, Scribner.
- Hanaor, A., 1992. Aspects of design of double layer tensegrity domes. International Journal of Space Structures 7 (2), 101–113.
- Kenner, H., 2003. Geodesic Math and How to Use It. University of California Press, California.
- Linkwitz, K., 1999. Form-finding by the 'Direct Approach' and pertinent strategies for the conceptual design of prestressed and hanging structures. International Journal of Space Structures 14, 73–87.
- Masic, M., Skelton, R.E., Gill, P.E., 2005. Algebraic tensegrity form-finding. International Journal of Solids and Structures 42, 4833–4858.
- Pagitz, M., James, J., 2007. Symmetry transformation matrices for structures. Proceedings of the Royal Society A 463, 1563–1583.
- Pagitz, M., Pellegrino, S., 2007. Buckling pressure of pumpkin balloons. International Journal of Solids and Structures 44, 6963–6986.
- Pellegrino, S., 1986. Mechanics of kinematically indeterminate structures, Ph.D. Thesis, University of Cambridge.
- Pugh, A., 1976. An Introduction to Tensegrity. University of California Press, California.
- Schek, H.J., 1974. The force density method for form finding and computation of general networks. Journal of Computer Methods in Applied Mechanics and Engineering 3, 115–134.
- Snelson, K.D., 1965. Continuous Tension, Discontinuous Compression Structures, United States Patent 3169611.
- Sultan, C., 1999. Modeling, design and control of tensegrity structures with applications, Ph.D. Thesis, Purdue University.
- Sultan, C., Corless, M., Skelton, R.E., 1999. Reduced prestressability conditions for tensegrity systems. International Journal of Solids and Structures 14, 147–154.
- Tibert, A.G., 2003. Deployable Tensegrity Structures for Space Applications, Ph.D. Thesis, Royal Institute of Technology.
- Tibert, A.G., Pellegrino, S., 2003. Review of form-finding methods for tensegrity structures. International Journal of Solids and Structures 18 (4), 209–223.
- Vanderplaats, G.N., 2001. Numerical Optimization Techniques for Engineering Design. Vanderplaats Research & Development, Inc.